Double-layer distribution of hydronium and hydroxide ions in the air-water interface

Pengchao Zhang[1], **Muye Feng**[2], and **Xuefei Xu**[1,*].

[1]Center for Combustion Energy, Department of Energy and Power Engineering, and Key Laboratory for Thermal Science and Power Engineering of Ministry of Education, Tsinghua University, Beijing 100084, China

[2]School of Mechanical and Power Engineering, Nanjing Tech University, Nanjing 211816, China

[*]Corresponding author e-mail: xuxuefei@tsinghua.edu.cn

July 2, 2023

Abstract

The acid-base nature of the aqueous interface has long been controversial. Most macroscopic experiments suggest that the air-water interface is basic based on the detection of negative charges at the interface that indicates the enrichment of hydroxides (OH^-), whereas microscopic studies mostly support the acidic air-water interface with the observation of the hydronium (H_3O^+) accumulation in the top layer of the interface. It is crucial to clarify the interfacial preference of OH^- and H_3O^+ ions for rationalizing the debate. In this work, we perform deep potential molecular dynamics simulations to investigate the preferential distribution of OH^- and H_3O^+ ions at aqueous interfaces. The neural network potential energy surface is trained based on density functional theory calculations with the SCAN functional, which can accurately describe the diffusion of these two ions both in the interface and in the bulk water. In contrast to the previously reported single ion enrichment, we show that both OH^- and H_3O^+ surprisingly prefer to accumulate in interfaces, but at different interfacial depths, rendering a double-layer ionic distribution within ~1 nm below the Gibbs dividing surface. The H_3O^+ is preferentially adsorbed in the topmost layer of the interface, but the OH^-, which is enriched in the deeper interfacial layer, has a higher equilibrium concentration due to the more negative free energy of interfacial stabilization (–0.90 (OH^-) vs. –0.56 (H_3O^+) kcal/mol). The air-water interface is therefore negatively charged, in agreement with the macroscopic charge detection and not in contradiction with the microscopic studies. The present finding of the ionic double-layer distribution qualitatively offers a self-consistent explanation for the long-term controversy about the acid-base nature of the air-water interface.

1 Introduction

Aqueous interfaces are ubiquitous in nature and engineering applications. The acid-base chemistry of aqueous interfaces is critical in fields as diverse as biology, atmospheric science, geochemistry, and engineering.[1–3] The accumulated water self-ions, hydroxide OH^- and hydronium H_3O^+, at aqueous interfaces can not only influence the interfacial electrostatic but also directly participate in many interfacial physical and chemical processes. Great efforts have been devoted to exploring the preference of water self-ions in the interfaces, as well as their electronic and geometrical structures and dynamic properties for the deep understanding of the interfacial acid-base chemistry, especially for its role in the electrochemical processes.[4–6] However, the acid-base chemical characteristics near the interfaces are still elusive,[7] and even whether excess hydroxides and/or hydroniums accumulate in the air-water interface remains controversial.[8–10]

There has been extensive research into how water self-ions are attracted and distributed in the air-water interfaces.[8,11] The majority of macroscopic experiments indirectly determined the enrichment of OH^- ions and accordingly

regarded the aqueous interfaces as basic.[10] In 1861, the first electrophoretic test revealed that air bubbles in the water had a negative zeta potential.[12] Subsequently, it was extensively reported that O_2/N_2/air bubbles[13–15] and oil droplets[14,16,17] in water all exhibited the negative zeta potential. It was inferred that the measured negative zeta potential was caused by interfacial enrichment of OH^- because it is the only anionic source in neat water. In fact, the negative zeta potentials of bubbles and oil droplets were observed even under acidic conditions.[14,16,18] A spectroscopic study with the second harmonic generation technique provided evidence of OH^- adsorption at the hexadecane/water interface.[19] However, more surface-sensitive spectroscopic measurements with atomic resolution found an enhancement of hydronium ions at aqueous interfaces, indicating the acidity of the interfaces.[8,20,21] In addition, it was reported that compared to pure water, the macroscopic surface tension of the inorganic base solution increases, but that of the strong acid solution decreases, which was claimed to imply an enrichment of H_3O^+ in the air-water interface and an interfacial repulsion of the OH^- ions.[22,23]

On the other hand, the majority of microscopic simulations supported the acidic aqueous interfaces.[9] Most molecular dynamics (MD) simulations (including *ab initio* MD (AIMD) with Car-Parrinello[24] and Born-Oppenheimer[9] methods, and classical MD with thermodynamically consistent,[25] reactive,[26] and polarizable[27] force fields) of the water droplet and/or slab found that the H_3O^+ ions were tended to accumulate at the topmost layer of the interfaces, and the OH^- ions were repelled into the aqueous bulk.[26,27] The adsorption tendencies of H_3O^+ at interfaces were explained by the dipole orientation in the interfacial electric field[25] and a favorable enthalpic contribution,[26] and the repulsion propensities of OH^- at interfaces were interpreted as results of an enthalpic penalty[26] and a lower entropy.[27] While a few computational simulations (which also include both AIMD,[28,29] and MD with a reactive and polarizable force field[30]) obtained the opposite results, i.e., OH^- rather than H_3O^+ was observed to be slightly accumulated at the air-water interface.[28–30] The discrepancy between the simulation results may not only be due to the use of different simulation models and methods, but also due to the limited simulation scales in space and time.

Given the inconsistency of various measurements and simulations, a trade-off hypothesis that the aqueous interface is neutral at pH = ~3-4 (pK_w = ~6-8, rather than ~14 in the bulk water) was proposed,[8,31,32] i.e., the aqueous interface is both acidic and basic.[8] Nevertheless, to the best of our knowledge, this hypothesis has not been confirmed by either experiments or theoretical simulations.

It is worth pondering why these previous investigations gave conflicting results on the preference of water self-ions at aqueous interfaces. From the experimental aspect, there are two possible reasons: 1) Detection depths at the aqueous interface using various techniques are ambiguous,[11] which may have visited different micro-scale regions of the interface; 2) More advanced experimental techniques on the molecular scale are yet to be developed, and the in-operando detection of ion distribution at interfaces with the standard surface-science methods is still challenging.[33–35] To identify the acid-base nature of interfaces, most experimental studies today rely mainly on indirect measurements. In terms of theoretical computations, the modeling scale of accurate AIMD, which is usually limited to simulations for hundreds of water molecules and hundreds of picoseconds due to the expensive computational cost, is far from the actual interface scale and dynamic time scale, so it is possible that these simulation results were slightly deviated. Although classical MD can be applied to larger interfacial systems (including more than thousands of water molecules) for simulations at the nanosecond level, it is almost impossible to accurately describe the diffusion process of self-ions in water with most non-reactive force fields, because the reactive process of proton hopping in the Grotthuss mechanism[36,37] is expected to play an important role in the diffusion, which involves the formation and breakage of oxygen-hydrogen bonds and needs to be described with *ab initio* methods or advanced reactive/polarizable force fields.

To improve the microscopic understanding of the acid-base feature at aqueous interfaces from a computational perspective, a possible way is to combine the advantages of classical MD (fast computational speed) and AIMD (high accuracy of the potential energy surface (PES)). In recent years, deep learning has become an effective method for approximating high-dimensional functions and offered the possibility of fitting extremely sophisticated PESs. Since Blank et al. pioneered the neural network approach to describe potential energy surfaces,[38] many neural network-based PES fitting methods were subsequently introduced, including the high-dimensional neural network potential (HDNNP),[39] deep potential (DP),[40] and SchNet,[41] etc., which greatly improved the accuracy and efficiency of molecular dynamics simulations. Today, large-scale MD based on DP models (DPMD) has been successfully applied in a wide variety of studies involving interfacial[42–44] and many other materials science topics,[45] which is able to achieve *ab initio* level of accuracy and linear scaling with the number of atoms. Therefore, we are motivated to re-examine the distribution and diffusion of water self-ions at nanoscale interfaces using the DPMD method.

DP models for water systems have been well developed and applied for studying water properties, such as ice nucleation,[46] phase diagrams,[47] and nuclear quantum effects (NQEs).[48,49] In the present work, we trained a DP model capable of accurately describing the water self-ion diffusion and the hydrogen bond (HB) network both in the interface and the bulk water, based on density functional theory (DFT) calculations. Then we performed DPMD simulations for the water slab and droplet systems to investigate the distributions of OH^- and H_3O^+ in the interfaces and the bulk water. Unexpectedly, we observed a preferential accumulation of OH^- and H_3O^+ at different depths of the interface. By analyzing the diffusion processes, the distribution frequency profiles, the zeta potential, the free energy, the solvated ion structures, and the HB network of the self-ions, we qualitatively provide a mutually self-consistent explanation for the long-standing controversy on the air-water interfacial acid-base nature.

2 Method

2.1 Deep potential model

The DP model was trained with DeePMD-kit package,[40] based on the reference energy and force calculated by the strongly constrained and appropriately normed (SCAN) meta-generalized-gradient-approximation (meta-GGA) functional.[50] The SCAN functional was chosen because it has been demonstrated to be able to well describe the electrical, structural, and dynamic properties of water molecules and water self-ions in previous tests.[46–48,51–53]

To simulate the diffusion and population of water self-ions both in the bulk water and the air-water interface, the training dataset consists of a diverse set of configurations selected from bulk water and interface water, with or without containing self-ions. In detail, these datasets were generated by the concurrent learning scheme with DP Generator (DP-GEN),[54] which interactively performs three steps, namely, DP training by DeePMD-kit,[40] DPMD exploration by LAMMPS,[55] and SCAN labeling by VASP.[56,57] The initial training datasets used to start the DP-GEN workflows were taken from short-time AIMD trajectory simulations. In the DPMD exploration step, to fully sample the conformational space, various DPMD simulations (e.g., in canonical (NVT) and isothermal-isobaric (NPT) ensembles, for selected temperatures from 270 to 600 K and selected pressures from 0.2 to 10 bar) were carried out using the DP models trained in the previous loop. In the SCAN labeling step, the candidate configurations were chosen based on the maximal deviation of forces, which will be added to the current training dataset for the next loop.

After iterative training with DP-GEN, in total 10,914 and 7,344 frame configurations were collected for pure water and self-ions containing water systems, respectively. To be able to learn the features of the incomplete hydrogen bond network near the air-water interface, 400 additional frame configurations of the water slab systems from the AIMD trajectory are added to the final training dataset. The details of these datasets are given in Table S3. The final DP model gradually converges after 10 million steps with the learning rate from 10^{-3} to 10^{-8}. The trained DP model was validated for a variety of testing datasets with configurations also collected from short-time AIMD trajectories, which were completely independent of the training datasets.

2.2 DPMD simulations

With the final DP model, the diffusion processes and the interfacial preference of self-ions in water droplet and slab systems were investigated by using the DPMD method. Table 1 provides an overview of the configurational details of these simulation systems, and Fig. 1 displays their schematic diagrams. In the droplet systems, a water droplet with a diameter of 50 Å is placed in a periodic cube box with a side length of 80 Å, where the vacuum region is big enough to avoid the influence of periodic boundary conditions. Considering the existence of curvature at the droplet interface, larger and more generalized slab systems were constructed for comparison. In the slab systems, the thicknesses of the water and vacuum layers

Table 1: **Details of DPMD simulation systems.**

System	Box size (Å^3)	No. of H_2O	No. (Molar) of H_3O^+	No. (Molar) of OH^-
Droplet 1	$80 \times 80 \times 80$	2267	0	0
Droplet 2	$80 \times 80 \times 80$	2257	0	10 (0.25 M)
Droplet 3	$80 \times 80 \times 80$	2257	10 (0.25 M)	0
Slab 1	$41 \times 41 \times 300$	5500	0	0
Slab 2	$41 \times 41 \times 300$	5476	0	24 (0.24 M)
Slab 3	$41 \times 41 \times 300$	5476	24 (0.24 M)	0

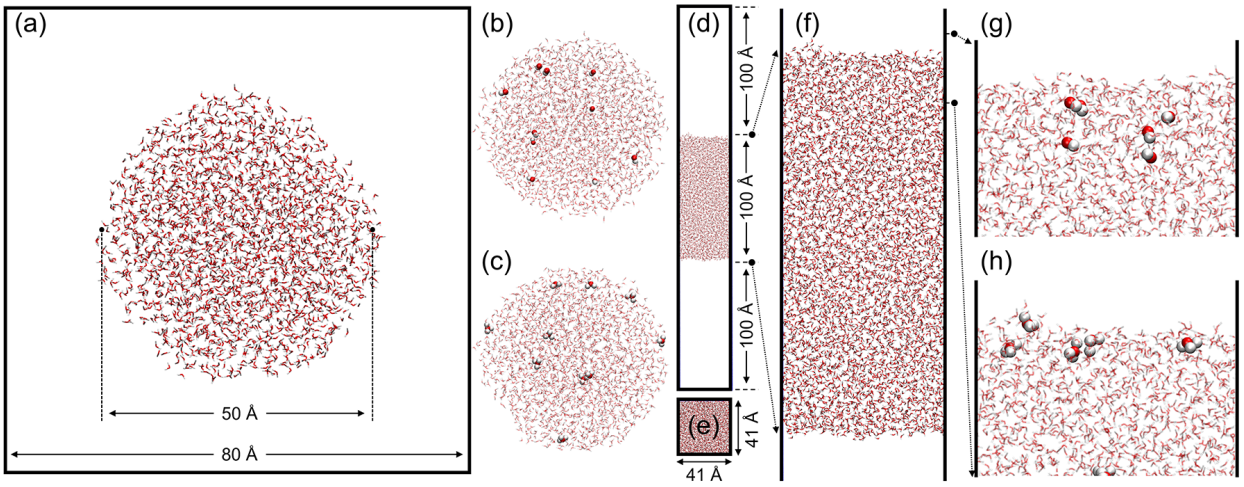

Figure 1: **Schematic diagrams of droplet and slab systems.** (a) Droplet 1: A pure water droplet located at the center of the periodic box; (b) Droplet 2: A hydroxides-containing water droplet; (c) Droplet 3: A hydroniums-containing water droplet; (d) The side view of slab systems; (e) The top view of slab systems; (f) The zoom-in side view of slab systems; (g) Hydroxides in the air-water interface of the Slab 2 system. (h) Hydroniums in the air-water interface of the Slab 3 system. The water self-ions are represented by the ball model, and the rest of the water molecules are represented by the stick model. The red and white colors represent the oxygen and hydrogen atoms, respectively.

are set to be 100 Å and 200 Å, respectively, which are adequate to create the nanoscale air-water interface.

All of the DPMD simulations were performed at 300 K in the NVT ensemble using the LAMMPS package,[55] and some slab systems were also simulated at 330 K to mimic the nuclear quantum effects[58] which were expected to accelerate the diffusion of water self-ions due to the quantum delocalization of protons. The temperatures were conserved with the Nosé-Hoover thermostat[59,60] using a damping time of 0.1 ps. In the initial state, the self-ions were randomly placed in all simulation systems. All trajectories were simulated for 30 ns with a timestep of 1 fs. The diffusions of water self-ions reached the dynamic equilibrium within the first 10 ns of the simulation, so the analysis was carried out based on the data of the last 20 ns with intervals of 1 ps for droplet systems and 4 ps for slab systems, respectively. The visualization of the simulation results is generated by VMD[61] and Matplotlib.[62] Post-processing of HB analysis is conducted using the MDAnalysis package.[63,64]

3 Results and discussion

3.1 Validation of the DP model

3.1.1 Comparison with the SCAN calculations

We first examined the validity of the trained DP model for the test dataset. Compared to the SCAN results (Fig. S2), the deviation of the DP model is typically less than 1.50 meV/atom in the absolute energy and less than 0.10 eV/Å in the atomic force. Specifically, the root mean square errors (RMSE) of energy and force are 0.67 meV/atom and 0.035 eV/Å for the pure water system, and 1.46 meV/atom and 0.038 eV/Å for the self-ion containing system, respectively. The high accuracy achieved on the test dataset indicates the adequacy of configurational sampling.

3.1.2 Performance in the prediction of structures and dynamic properties

We further tested the performance of the DP model in predicting the water structure and the dynamic properties of water self-ions. The radial distribution functions (RDFs) of the pure water system obtained from DPMD simulation were compared with those from AIMD. As shown in Fig. S4, the RDF curves of DPMD and AIMD agree very well, reflecting the accuracy of the DP model in describing the water structure.

The dynamical self-ion diffusion process in water has been extensively studied theoretically[36,65,66] and experimentally.[67] It is widely accepted that the proton diffusion in water follows the Grotthuss mechanism,[37] where the proton forms water wires with neighboring water molecules, and the H_3O^+ diffusion is achieved by rapid transitions between Eigen and Zundel configurations. Our DPMD simulations also observed the proton diffusion path following the Grotthuss mechanism. As shown in Fig. 2(a-c), the structural diffusion process of H_3O^+ is achieved by the interconversion of two Eigen con-

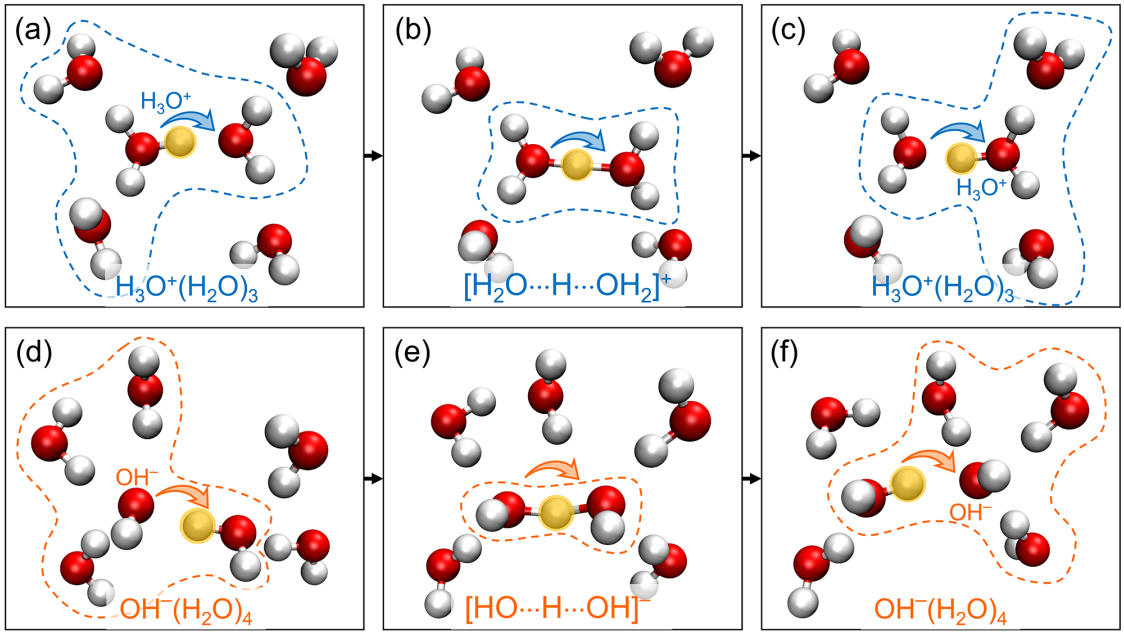

Figure 2: **Schematic diagrams of hydronium and hydroxide diffusion.** (a-c) hydronium and (d-f) hydroxide diffusion processes are extracted from the DPMD simulations of slab systems. The transferring protons are shaded in yellow, and the direction of self-ion diffusion is marked by arrows.

figurations ($H_3O^+(H_2O)_3$) via an intermediate Zundel configuration ($[H_2O\cdots H\cdots OH_2]^+$). And we discovered the OH^- diffusion processes with the help of proton hopping in our DPMD simulations, as same as that reported by the previous AIMD study.[36,65,66] That is, from an initial state of OH^- in coordination with four adjacent water molecules ($OH^-(H_2O)_4$, see Fig. 2(d)), the water coordination number of OH^- is firstly reduced to form $[HO\cdots H\cdots OH]^-$ (Fig. 2(e)), and then the centered proton hops between the two oxygen atoms due to the thermodynamic fluctuation. Ultimately, OH^- completes the structural diffusion into another fourfold-coordinated $OH^-(H_2O)_4$ solvent structure and waits for the next proton hopping (Fig. 2(f)). In addition, the diffusion coefficients extracted from our SCAN-based DPMD simulations are 6.0×10^{-9} and 3.0×10^{-9} m^2s^{-1} for H_3O^+ and OH^- at 330 K, respectively, as shown in Table S4, which are slightly smaller than the experimental measurement (~9×10^{-9} m^2s^{-1} for H_3O^+ and ~5×10^{-9} m^2s^{-1} for OH^- at ~300 K)[68–70] but agree well with those obtained by CPMD simulations with the SCAN functional (5.7×10^{-9} m^2s^{-1} for H_3O^+ and 2.9×10^{-9} m^2s^{-1} for OH^- at 330 K).[51] The obtained diffusion coefficients are sufficient to achieve a dynamic equilibrium state in our 30 ns simulations. Thus, we demonstrated the reliability of the DP model in studying the structural and dynamical properties of water self-ions.

3.2 Distribution of hydroxide and hydronium at the air-water interface

3.2.1 Double-layer distribution

Using the validated DP model, we carried out the DPMD simulations to investigate the equilibrium distribution of water self-ions in several systems (Droplet 2, Droplet 3, Slab 2, and Slab 3). No matter for a droplet or a slab system, the evolution of the positions of these ions with simulation time demonstrates that the dynamical equilibria of the diffusion processes (Fig. S5 and Fig. S6) are all reached after 0-10 ns. As shown in Fig. 3(a-b), the statistical analysis in the equilibrium interval (10-30 ns) reveals that the maxima of ion distribution frequencies for both hydroxide- and hydronium-containing systems appear within ~1 nm below the average Gibbs dividing surface (GDS), where mass density is half that of the bulk water.[6,26,28,42] (The region close to the GDS can be considered as the air-water interface.) In particular, H_3O^+ primarily locates at 1.0 Å below the GDS in all systems (the topmost layer of the interface), and OH^- mainly accumulates at a depth of 4.9 Å below the GDS. These results indicate that both water self-ions prefer to accumulate in the air-water interface rather than in the bulk at 300 K.

When the temperature is increased to 330 K (Fig. 3(c)), the distributions of both ions in the slab systems become slightly more delocalized as compared to 300 K, espe-

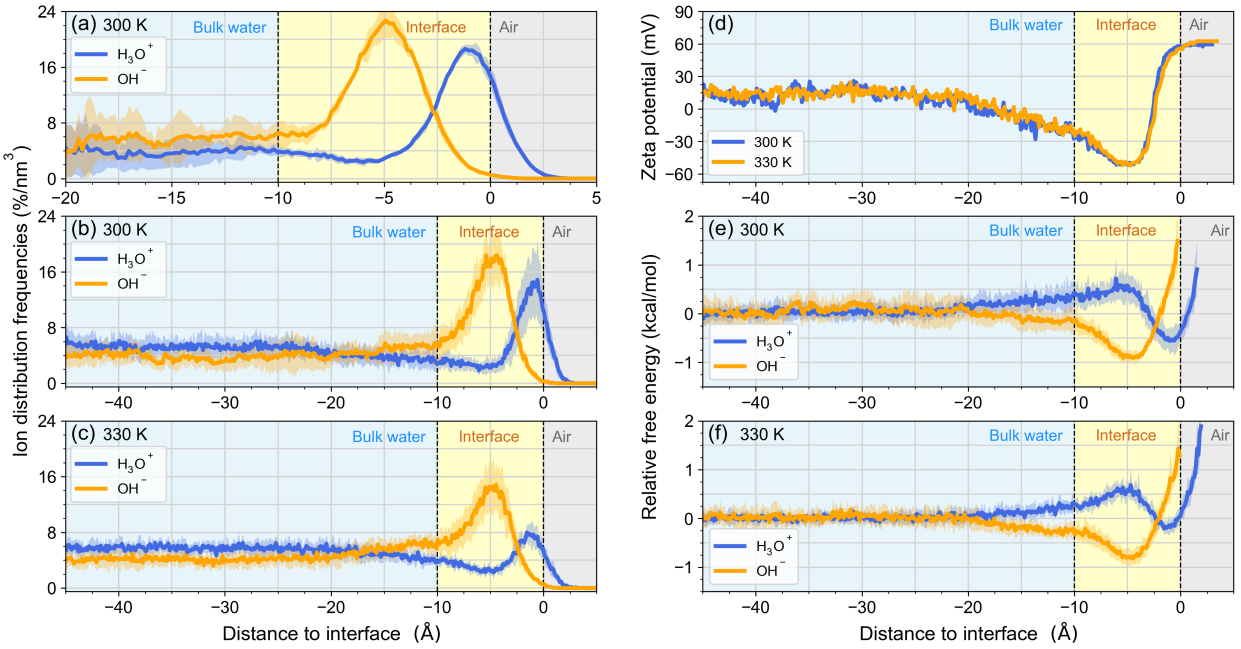

Figure 3: **Ionic distribution frequency, zeta potential and free energy.** Volume normalized distribution frequencies of hydroxide and hydronium as functions of normal distance to the air-water interface in (a) Droplet 2 and Droplet 3 systems at 300 K, (b) Slab 2 and Slab 3 systems at 300 K, and (c) Slab 2 and Slab 3 systems at 330 K. The distribution frequency is calculated as the ratio of the number of ions presenting in the defined region to the total number of ions. (d) The zeta potentials of slab systems are estimated based on the distribution frequencies. Relative free energy profiles of hydroxide and hydronium in Slab 2 and Slab 3 systems at (f) 300 K and (g) 330 K. The normal distances to the interface are defined as negative on the liquid side, zero at GDS, and positive on the air side. The transparent shading represents the standard deviation. The regions of bulk water, interface, and air are distinguished by different colored backgrounds.

cially for hydroniums, which show a weak dependence of the distribution frequency on the normal distance to the interface, but their peaks are still located close to the GDS at different interfacial depths and still have a separation of ~4 Å. Although the distribution peaks of both ions are lowered as compared to those at 300 K, their relative height difference is increased. We can see a significantly higher distribution frequency peak of OH^- than that of H_3O^+, indicating much more accumulation of OH^- than H_3O^+ at the air-water interface. In addition, Fig. 3(c) demonstrates that the minimum distribution of H_3O^+ and maximum distribution of OH^- coincide at the same interfacial depth. It implies a double-layer distribution of water self-ions at the air-water interface in the neutral, weakly basic, and weakly acidic systems.

Note that in the present simulations, we did not include the NQEs. It has been reported that the NQEs can soften the water structure by destabilizing the hydrogen bonding network,[58] which is partially similar to the temperature effect. Hence, it is speculated that if NQEs are considered, the ion distribution at 300 K could be closer to that we obtained at 330 K, i.e., when hydronium and hydroxide ions coexist in water, there could be an apparent ionic double-layer distribution with a gap of ~4 Å in the air-water interface, in which H_3O^+ is in the top layer of the interface but OH^- in the lower layer accumulate much more intensively than H_3O^+. This explains why the macroscopic experiments determined the negative charge enrichment at the aqueous interface.

3.2.2 Interfacial free energies and zeta potentials

The free energy and zeta potential profiles of the water self-ions as functions of interfacial depths were calculated based on the simulated distribution probabilities for the Slab 2 and Slab 3 systems. As depicted in Fig. 3(e-f), the free energy profile of H_3O^+ has a minimum at ~1.0 Å below the GDS, which is also the depth with the maximum H_3O^+ population. This minimum free energy is 0.56 ± 0.24 (0.19 ± 0.08) kcal/mol lower than that in the bulk at 300 (330) K, in reasonable agreement with the interfacial stabilization energy of −1.3 ± 0.2 kcal/mol observed experimentally[21] and with the previously sim-

ulated values –0.55 kcal/mol,[26] –0.60 kcal/mol,[25] and -1.0 ± 0.2 kcal/mol[42] at 300 K. Similarly, for OH^-, at the depth of 4.9 Å below the GDS with the maximum population, we also get the lowest free energy, and thus the interfacial stabilization energy of OH^- is determined to be −0.90 ± 0.10 (−0.81 ± 0.14) kcal/mol at 300 (330) K. The previous simulations predicted slightly smaller interfacial stabilization energies for OH^-, which were –0.6 kcal/mol[29] and –0.5 kcal/mol[28] at 300 K.

We also notice that there is a free energy barrier for hydronium diffusion from its optimal distribution depth (1 Å below the GDS) to the bulk, which is 1.13 ± 0.25 (0.81 ± 0.18) kcal/mol at 300 (330) K, and the barrier is coincidentally located at the position (4.9 Å below the GDS) with the lowest free energy of OH^-. All these results indicate that the interface has stronger adsorption to OH^- than to H_3O^+, that H_3O^+ tends to be enriched in the topmost layer of the interface, and that once these self-ions are adsorbed in their optimal interfacial position, they have to overcome a free energy barrier of ~1 kcal/mol to diffuse back into the bulk. This means that the double-layer distribution is dynamically stable. The relatively weaker interfacial stabilization energy of H_3O^+ than OH^- also determines the lower H_3O^+ population at the interface. This is why we observe a higher distribution frequency peak for OH^- than for H_3O^+.

As shown in Fig. 3(c), a positive zeta potential (~60 mV) and a negative zeta potential (~–50 mV) are respectively predicted at depths with the maximum populations of H_3O^+ and OH^-. We further estimate the interfacial zeta potential of the neutral water by assuming the interface with a thickness of 1 nm (the air-water interface thickness has been estimated to be 0.3-1 nm[71–73]) and by simply accounting for all ionic distribution near the GDS (from interfacial depth –7.5 Å to 2.5 Å with the GDS as zero point) in the Slab 2 and Slab 3 systems, and we get an interfacial zeta potential of –13 mV (–23 mV) at 300 K (330 K), which supports the experimental observation of negative zeta potential for O_2/N_2/air bubbles[13–15] and oil droplets.[14,16,17]

3.2.3 Rethink of the controversy on the interfacial preference of self-ions

As far as we know, this finding, that the H_3O^+ and OH^- both prefer to accumulate in the air-water interface but at different depths and with a distinction of concentration, has not been fully recognized. As we mentioned in the introduction section, some previous simulations revealed the adsorption propensity of H_3O^+ at the topmost interfacial layer,[9,24–27] but others also provided evidence of the slight enhancement of OH^- at the interface[28–30] with H_3O^+ avoiding the interface[30] or equally distributing at the interface and in the bulk water.[28] They have come to contradictory conclusions, as have the experimental measurements, so the debate never ends. The present direct observation - the double-layer distribution of hydronium and hydroxide ions at the interface - may help to understand the long-standing controversy about the interfacial propensity of water self-ions. In fact, the speculation of the double-layer distribution had been proposed and discussed by a few groups.[8,10,14] Unfortunately, it did not obtain much attention due to the lack of direct evidence. The present work shows that the separation of two ionic layers at the interface is only about 4 Å, which is so narrow that it is difficult to be recognized experimentally.

Based on our simulations, we draw schematic diagrams of the ionic double-layer distribution at the air-water interface in Fig. 4 for three circumstances, a water slab, a water droplet, and an air (or vacuum) bubble in water, in order to understand the experimental observations. Both OH^- and H_3O^+ in water are attracted toward the interface to form the double-layer distribution with a thickness of ~1 nm, where the H_3O^+ layer is closer to the air (or vacuum) side as compared to the OH^- layer and has a lower ionic concentration due to the lower interfacial stabilization free energy. Thus, the net charge of the interface should be negative, and a negative zeta potential is measured in the macroscopic experiments, which has been confirmed by our estimation for the interfacial zeta potential of the neutral water in the above section. While the microscopic spectroscopic experiments could give opposite results if they detected different interfacial depths, for example, if the detection depth only reaches the topmost layer of the interface, these atomic level experiments will find the enrichment of H_3O^+, but if they go a little deeper they might see the OH^- layer.

In addition, note that the air-water interfaces of a water droplet in the air (Fig. 4(c)) and an air bubble in the water (Fig. 4(d)) are both negatively charged, but the structures of the double-layer distribution are opposite due to the different curvature orientation of gas and liquid phases.

3.3 Reason for the water self-ionic double-layer distribution in the interface

Next, we further discuss the intrinsic reason for the double-layer distribution of water self-ions in the air-water interface.

In the microscopic view, the orientation distributions (Fig. 5(a-b)) of OH^- ($\cos\theta$ = –1.0 - 1.0) and H_3O^+ ($\cos\theta$ = ~1.0) at the interface are distinctly different, where the orientation is defined by the cosine of θ angle between the normal vector of the air-water interface and the dipole

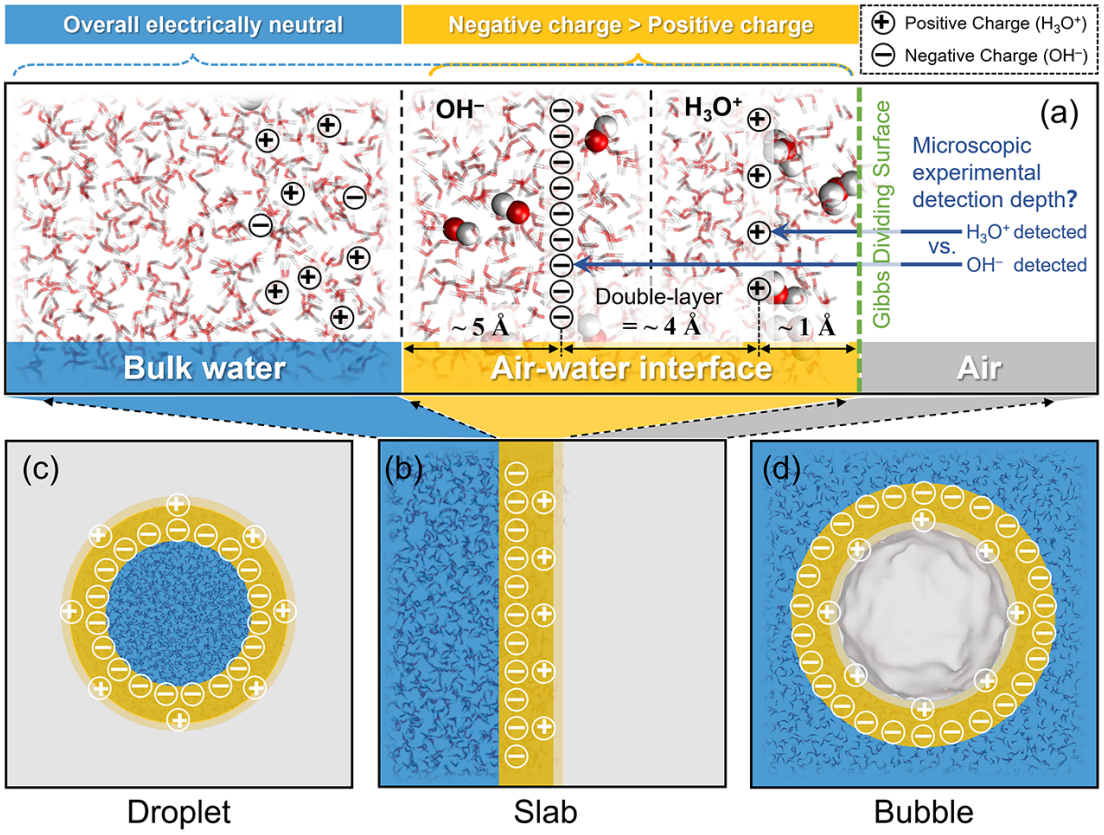

Figure 4: **Schematic diagram of double-layer distribution in the air-water interfaces.** The zoom-in self-ionic double-layer distribution of (a) the slab system in neutral water. The schematic double-layer distribution in the systems of (b) the water slab, (c) the water droplet in air, and (d) the air (or vacuum) bubble in water.

vector of ions (Fig. 5(c-d)). Fig. 5(a) shows that the normal vector of the air-water interface and the dipole vector of H_3O^+ almost overlap, indicating that H_3O^+ ions mainly lie flat on the water surface with the hydrophobic oxygen atom facing the air. The three hydrophilic protons of H_3O^+ can form three hydrogen bonds with three neighboring water molecules (Fig. 5(f) and Fig. 5(i)), which is consistent with previous works.[25,74,75] In this orientation, H_3O^+ is more stable at the topmost layer of the interface because its hydrophobic oxygen, which hardly acts as an HB acceptor (Fig. 5(j)) due to having fewer lone pair electrons, is pushed towards the interface to keep a better HB network of the bulk water. It also explains why the temperature effect and the nuclear quantum effect, both of which soften the HB network, will weaken the interfacial preference of H_3O^+, as we observed in Fig. 3.

Similar to the hydronium, OH^- also has amphiphilic behaviors.[51,70,76] Considering this, one could assume that the orientation of OH^- in the air-water interface might be like that of H_3O^+, i.e., the hydrophilic oxygen towards the liquid phase and the hydrophobic hydrogen towards the gas phase. However, the fact is that such conformations ($\cos\theta = -1.0$) account for only a small fraction as depicted in Fig. 5(a). This is because the hydrophobic hydrogen of OH^- can also act as the HB donor to interact with one water molecule (Fig. 5(g)), leading to the relatively weaker hydrophobicity of OH^- than H_3O^+. The hydrophilic oxygen, which has more lone pair electrons than the oxygen of neutral water molecule, can act as an HB acceptor to form HBs with 3-5 water molecules[27,66,76] (see Fig. 5(e) and Fig. 5(h)). The abundant HB network arises from the delocalization of oxygen lone pair electrons, forming a stable dynamic hyper-coordination solvation structure of OH^-,[66,76] so that the orientation of OH^- is randomly distributed.

Although the OH^- can form more HBs than H_3O^+, it also weakens the overall HB network of bulk water as shown in Fig. 5(k-l), and consequently it is attracted to the interface with the partially broken HB network to reduce the disruption to the HB structure of bulk water. At the same time, the hyper-coordination solvation structure of OH^- keeps it away from the topmost layer of the

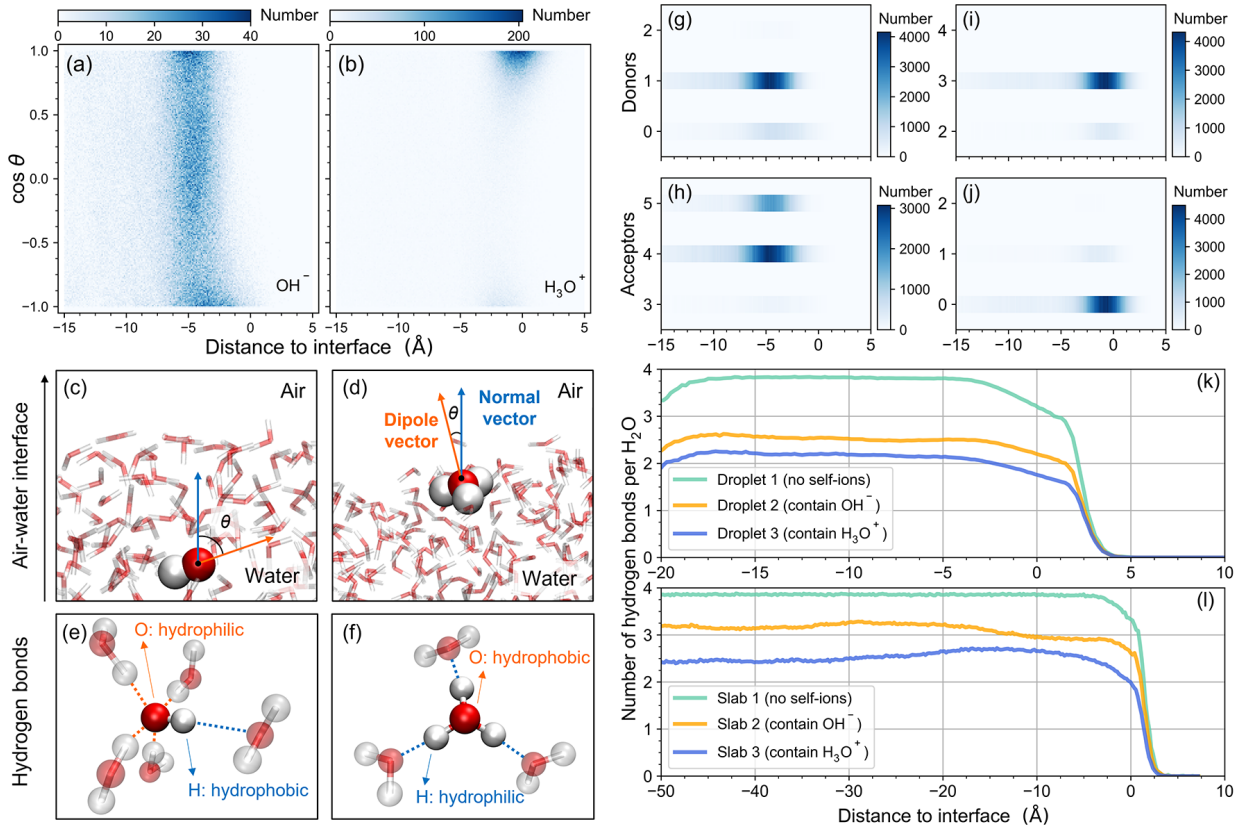

Figure 5: **The solvation structures and the hydrogen bond network of water self-ions in the air-water interface.** The orientation distributions of (a) hydroxide in the Droplet 2 system and (b) hydronium in the Droplet 3 system at 300 K. The color bars represent the cumulative number of hydroxides or hydroniums in statistical intervals. The orientation is defined by the cosine of θ angle between the normal vector of the air-water interface and the dipole vector (from H to O) of the (c) hydroxide or (d) hydronium. (e) and (f) are schematic diagrams of HBs around the amphiphilic hydroxide and hydronium, where the blue and orange dashed lines represent the self-ions being the HB donors and acceptors, respectively. The numbers of acting (g) as HB donors and (h) as HB acceptors for each hydroxide in the Droplet 2 system, and the numbers of acting (i) as HB donors and (j) as HB acceptors for each hydronium in the Droplet 3 system along various interfacial depths at 300 K, where the color bars represent the cumulative number of donors or acceptors in statistical intervals. The average number of HBs per water molecule as functions of normal distance to the air-water interface in (k) droplet systems and (l) slab systems at 300 K.

interface (where H_3O^+ is preferentially adsorbed), and instead OH^- prefers to accumulate at the interfacial depth of 2-4 water-molecule layers below the GDS (Fig. 5(c)). Thus, the double-layer distribution of water self-ions in the interfaces can eventually form when thermodynamic equilibrium is reached.

4 Conclusion

In this work, we trained an accurate deep potential model for hydroxide- and hydronium-containing water systems based on the density functional theory calculations with the SCAN functional, and then performed DPMD simulations to study the distribution of water self-ions in water droplet and slab systems. We found that both OH^- and H_3O^+ tend to accumulate in the air-water interface but at a different depth, leading to an ionic double-layer distribution at the interface. The interfacial propensity arises from the amphipathy of the water self-ions; the distinct stable solvation structures determine that they are preferentially adsorbed at different interfacial depths: H_3O^+ with a strongly hydrophobic oxygen atom is closer to the water surface, in agreement with most microscopic studies, OH^- with a hyper-coordination solvation structure prefers to locate at a deeper interfacial depth, and the gap between the two ion layers is only ~4Å. As compared to H_3O^+, OH^- has a higher interfacial stabilization free energy and consequently a higher concentration in the

interface. It explains the negatively charged air-water interface observed in macroscopic experiments. Thus, our results qualitatively provide a self-consistent explanation for the long-standing controversy between previous macroscopic and microscopic studies on the interfacial distribution of water self-ions in the air-water interface.

Associated Content

Supporting Information contains DP model training and dataset building, validation of the DP model, distribution of the hydroxide and hydronium, zeta potential calculations, free energy calculations, and hydrogen bonding network of hydroxide and hydronium.

Acknowledgments

The authors are very grateful to professor Michele Parrinello, professor Xiao He and Axel Tosello Gardini for helpful discussion. This work was supported in part by the National Natural Science Foundation of China (Grant Nos. 21973053 and 52106164). A part of the computation was completed at the High Performance Computing Platform of Tsinghua University.

Author contributions

All authors participated in the design of the study. The collection of the training dataset was performed by P.Z. and M.F. The simulation and data analysis were performed by P.Z. Throughout all stages of the project, X.X. provided essential supervision. The first draft of the manuscript was prepared by P.Z. and subsequent revisions were carried out by all authors.

References

[1] Wei, Z.; Li, Y.; Cooks, R. G.; Yan, X. Accelerated reaction kinetics in microdroplets: Overview and recent developments. *Annual Review of Physical Chemistry* **2020**, *71*, 31–51.

[2] Ruiz-Lopez, M. F.; Francisco, J. S.; Martins-Costa, M. T.; Anglada, J. M. Molecular reactions at aqueous interfaces. *Nature Reviews Chemistry* **2020**, *4*, 459–475.

[3] Bjoörneholm, O.; Hansen, M. H.; Hodgson, A.; Liu, L.-M.; Limmer, D. T.; Michaelides, A.; Pedevilla, P.; Rossmeisl, J.; Shen, H.; Tocci, G., et al. Water at interfaces. *Chemical reviews* **2016**, *116*, 7698–7726.

[4] Li, Y.; Chen, Y.-X.; Liu, Z.-F. $OH^- \cdots$ Au Hydrogen Bond and Its Effect on the Oxygen Reduction Reaction on Au (100) in Alkaline Media. *The Journal of Physical Chemistry Letters* **2022**, *13*, 9035–9043.

[5] Zhong, G.; Cheng, T.; Shah, A. H.; Wan, C.; Huang, Z.; Wang, S.; Leng, T.; Huang, Y.; Goddard III, W. A.; Duan, X. Determining the hydronium pK_α at platinum surfaces and the effect on pH-dependent hydrogen evolution reaction kinetics. *Proceedings of the National Academy of Sciences* **2022**, *119*, e2208187119.

[6] Martins-Costa, M. T.; Ruiz-López, M. F. Electrostatics and Chemical Reactivity at the Air–Water Interface. *Journal of the American Chemical Society* **2023**,

[7] Noam, A.; Kramer, C. R.; Peter, P.; Sylvie, R.; Martin, T.; Ali, H., et al. Protons and Hydroxide Ions in Aqueous Systems. **2016**,

[8] Vácha, R.; Buch, V.; Milet, A.; Devlin, J. P.; Jungwirth, P. Autoionization at the surface of neat water: is the top layer pH neutral, basic, or acidic? *Physical Chemistry Chemical Physics* **2007**, *9*, 4736–4747.

[9] Buch, V.; Milet, A.; Vácha, R.; Jungwirth, P.; Devlin, J. P. Water surface is acidic. *Proceedings of the National Academy of Sciences* **2007**, *104*, 7342–7347.

[10] Beattie, J. K.; Djerdjev, A. M.; Warr, G. G. The surface of neat water is basic. *Faraday discussions* **2009**, *141*, 31–39.

[11] Saykally, R. J. Two sides of the acid–base story. *Nature chemistry* **2013**, *5*, 82–84.

[12] Quincke, G. Ueber die Fortführung materieller Theilchen durch strömende Elektricität. *Annalen der Physik* **1861**, *189*, 513–598.

[13] Graciaa, A.; Morel, G.; Saulner, P.; Lachaise, J.; Schechter, R. The ζ-potential of gas bubbles. *Journal of Colloid and Interface Science* **1995**, *172*, 131–136.

[14] Creux, P.; Lachaise, J.; Graciaa, A.; Beattie, J. K.; Djerdjev, A. M. Strong specific hydroxide ion binding at the pristine oil/water and air/water interfaces. *The Journal of Physical Chemistry B* **2009**, *113*, 14146–14150.

[15] Creux, P.; Lachaise, J.; Graciaa, A.; Beattie, J. K. Specific cation effects at the hydroxide-charged air/water interface. *The Journal of Physical Chemistry C* **2007**, *111*, 3753–3755.

[16] Marinova, K.; Alargova, R.; Denkov, N.; Velev, O.; Petsev, D.; Ivanov, I.; Borwankar, R. Charging of oil- water interfaces due to spontaneous adsorption of hydroxyl ions. *Langmuir* **1996**, *12*, 2045–2051.

[17] Beattie, J. K.; Djerdjev, A. M. The pristine oil/water interface: Surfactant-free hydroxide-charged emulsions. *Angewandte Chemie International Edition* **2004**, *43*, 3568–3571.

[18] Takahashi, M. ζ potential of microbubbles in aqueous solutions: electrical properties of the gas- water interface. *The Journal of Physical Chemistry B* **2005**, *109*, 21858–21864.

[19] Fang, H.; Wu, W.; Sang, Y.; Chen, S.; Zhu, X.; Zhang, L.; Niu, Y.; Gan, W. Evidence of the adsorption of hydroxide ion at hexadecane/water interface from second harmonic generation study. *Rsc Advances* **2015**, *5*, 23578–23585.

[20] Petersen, P. B.; Saykally, R. J. Evidence for an enhanced hydronium concentration at the liquid water surface. *The Journal of Physical Chemistry B* **2005**, *109*, 7976–7980.

[21] Das, S.; Imoto, S.; Sun, S.; Nagata, Y.; Backus, E. H.; Bonn, M. Nature of excess hydrated proton at the water–air interface. *Journal of the American Chemical Society* **2019**, *142*, 945–952.

[22] Jungwirth, P.; Tobias, D. J. Specific ion effects at the air/water interface. *Chemical reviews* **2006**, *106*, 1259–1281.

[23] Weissenborn, P. K.; Pugh, R. J. Surface tension of aqueous solutions of electrolytes: relationship with ion hydration, oxygen solubility, and bubble coalescence. *Journal of colloid and interface science* **1996**, *184*, 550–563.

[24] Lee, H.-S.; Tuckerman, M. E. *ab initio* Molecular Dynamics Studies of the Liquid-Vapor Interface of an HCl Solution. *The Journal of Physical Chemistry A* **2009**, *113*, 2144–2151.

[25] Mamatkulov, S. I.; Allolio, C.; Netz, R. R.; Bonthuis, D. J. Orientation-induced adsorption of hydrated protons at the air–water interface. *Angewandte Chemie International Edition* **2017**, *56*, 15846–15851.

[26] Tse, Y.-L. S.; Chen, C.; Lindberg, G. E.; Kumar, R.; Voth, G. A. Propensity of hydrated excess protons and hydroxide anions for the air–water interface. *Journal of the American Chemical Society* **2015**, *137*, 12610–12616.

[27] Hub, J. S.; Wolf, M. G.; Caleman, C.; van Maaren, P. J.; Groenhof, G.; van der Spoel, D. Thermodynamics of hydronium and hydroxide surface solvation. *Chemical Science* **2014**, *5*, 1745–1749.

[28] Baer, M. D.; Kuo, I.-F. W.; Tobias, D. J.; Mundy, C. J. Toward a unified picture of the water self-ions at the air–water interface: A density functional theory perspective. *The Journal of Physical Chemistry B* **2014**, *118*, 8364–8372.

[29] Mundy, C. J.; Kuo, I.-F. W.; Tuckerman, M. E.; Lee, H.-S.; Tobias, D. J. Hydroxide anion at the air–water interface. *Chemical Physics Letters* **2009**, *481*, 2–8.

[30] Bai, C.; Herzfeld, J. Surface propensities of the self-ions of water. *ACS central science* **2016**, *2*, 225–231.

[31] Colussi, A. J.; Enami, S.; Ishizuka, S. Hydronium ion acidity above and below the Interface of aqueous microdroplets. *ACS Earth and Space Chemistry* **2021**, *5*, 2341–2346.

[32] Mishra, H.; Enami, S.; Nielsen, R. J.; Stewart, L. A.; Hoffmann, M. R.; Goddard III, W. A.; Colussi, A. J. Brønsted basicity of the air–water interface. *Proceedings of the National Academy of Sciences* **2012**, *109*, 18679–18683.

[33] Zaera, F. Probing liquid/solid interfaces at the molecular level. *Chemical reviews* **2012**, *112*, 2920–2986.

[34] Goodman, D. W. Model studies in catalysis using surface science probes. *Chemical Reviews* **1995**, *95*, 523–536.

[35] Somorjai, G. A.; Park, J. Y. Molecular surface chemistry by metal single crystals and nanoparticles from vacuum to high pressure. *Chemical Society Reviews* **2008**, *37*, 2155–2162.

[36] Marx, D. Proton transfer 200 years after von Grotthuss: Insights from *ab initio* simulations. *ChemPhysChem* **2006**, *7*, 1848–1870.

[37] von Grotthuß, T. *Mémoire sur la décomposition de l'eau et des corps qu'elle tient en dissolution à l'aide de l'électricité galvanique*; 1805.

[38] Blank, T. B.; Brown, S. D.; Calhoun, A. W.; Doren, D. J. Neural network models of potential energy surfaces. *The Journal of chemical physics* **1995**, *103*, 4129–4137.

[39] Behler, J.; Parrinello, M. Generalized neural-network representation of high-dimensional potential-energy surfaces. *Physical review letters* **2007**, *98*, 146401.

[40] Wang, H.; Zhang, L.; Han, J.; Weinan, E. DeePMD-kit: A deep learning package for many-body potential energy representation and molecular dynamics. *Computer Physics Communications* **2018**, *228*, 178–184.

[41] Schütt, K. T.; Sauceda, H. E.; Kindermans, P.-J.; Tkatchenko, A.; Müller, K.-R. Schnet–a deep learning architecture for molecules and materials. *The Journal of Chemical Physics* **2018**, *148*, 241722.

[42] de la Puente, M.; David, R.; Gomez, A.; Laage, D. Acids at the Edge: Why Nitric and Formic Acid Dissociations at Air–Water Interfaces Depend on Depth and on Interface Specific Area. *Journal of the American Chemical Society* **2022**, *144*, 10524–10529.

[43] Galib, M.; Limmer, D. T. Reactive uptake of N_2O_5 by atmospheric aerosol is dominated by interfacial processes. *Science* **2021**, *371*, 921–925.

[44] Andrade, M. F. C.; Ko, H.-Y.; Zhang, L.; Car, R.; Selloni, A. Free energy of proton transfer at the water–TiO_2 interface from *ab initio* deep potential molecular dynamics. *Chemical Science* **2020**, *11*, 2335–2341.

[45] Wen, T.; Zhang, L.; Wang, H.; Weinan, E.; Srolovitz, D. J. Deep potentials for materials science. *Materials Futures* **2022**,

[46] Piaggi, P. M.; Weis, J.; Panagiotopoulos, A. Z.; Debenedetti, P. G.; Car, R. Homogeneous ice nucleation in an *ab initio* machine-learning model of water. *Proceedings of the National Academy of Sciences* **2022**, *119*, e2207294119.

[47] Zhang, L.; Wang, H.; Car, R.; Weinan, E. Phase diagram of a deep potential water model. *Physical review letters* **2021**, *126*, 236001.

[48] Xu, J.; Zhang, C.; Zhang, L.; Chen, M.; Santra, B.; Wu, X. Isotope effects in molecular structures and electronic properties of liquid water via deep potential molecular dynamics based on the SCAN functional. *Physical Review B* **2020**, *102*, 214113.

[49] Ko, H.-Y.; Zhang, L.; Santra, B.; Wang, H.; E, W.; DiStasio Jr, R. A.; Car, R. Isotope effects in liquid water via deep potential molecular dynamics. *Molecular Physics* **2019**, *117*, 3269–3281.

[50] Sun, J.; Ruzsinszky, A.; Perdew, J. P. Strongly constrained and appropriately normed semilocal density functional. *Physical review letters* **2015**, *115*, 036402.

[51] Liu, R.; Zhang, C.; Liang, X.; Liu, J.; Wu, X.; Chen, M. Structural and dynamic properties of solvated hydroxide and hydronium ions in water from *ab initio* modeling. *The Journal of Chemical Physics* **2022**, *157*, 024503.

[52] Zheng, L.; Chen, M.; Sun, Z.; Ko, H.-Y.; Santra, B.; Dhuvad, P.; Wu, X. Structural, electronic, and dynamical properties of liquid water by *ab initio* molecular dynamics based on SCAN functional within the canonical ensemble. *The Journal of Chemical Physics* **2018**, *148*, 164505.

[53] Chen, M.; Ko, H.-Y.; Remsing, R. C.; Calegari Andrade, M. F.; Santra, B.; Sun, Z.; Selloni, A.; Car, R.; Klein, M. L.; Perdew, J. P., et al. *ab initio* theory and modeling of water. *Proceedings of the National Academy of Sciences* **2017**, *114*, 10846–10851.

[54] Zhang, Y.; Wang, H.; Chen, W.; Zeng, J.; Zhang, L.; Wang, H.; Weinan, E. DP-GEN: A concurrent learning platform for the generation of reliable deep learning based potential energy models. *Computer Physics Communications* **2020**, *253*, 107206.

[55] Plimpton, S. Fast parallel algorithms for short-range molecular dynamics. *Journal of computational physics* **1995**, *117*, 1–19.

[56] Kresse, G.; Furthmüller, J. Efficient iterative schemes for *ab initio* total-energy calculations using a plane-wave basis set. *Physical review B* **1996**, *54*, 11169.

[57] Kresse, G.; Furthmüller, J. Efficiency of ab-initio total energy calculations for metals and semiconductors using a plane-wave basis set. *Computational materials science* **1996**, *6*, 15–50.

[58] Morrone, J. A.; Car, R. Nuclear quantum effects in water. *Physical review letters* **2008**, *101*, 017801.

[59] Nosé, S. A unified formulation of the constant temperature molecular dynamics methods. *The Journal of chemical physics* **1984**, *81*, 511–519.

[60] Hoover, W. G. Canonical dynamics: Equilibrium phase-space distributions. *Physical review A* **1985**, *31*, 1695.

[61] Humphrey, W.; Dalke, A.; Schulten, K. VMD: visual molecular dynamics. *Journal of molecular graphics* **1996**, *14*, 33–38.

[62] Hunter, J. D. Matplotlib: A 2D graphics environment. *Computing in science & engineering* **2007**, *9*, 90–95.

[63] Michaud-Agrawal, N.; Denning, E. J.; Woolf, T. B.; Beckstein, O. MDAnalysis: a toolkit for the analysis of molecular dynamics simulations. *Journal of computational chemistry* **2011**, *32*, 2319–2327.

[64] Gowers, R. J.; Linke, M.; Barnoud, J.; Reddy, T. J.; Melo, M. N.; Seyler, S. L.; Domanski, J.; Dotson, D. L.; Buchoux, S.; Kenney, I. M., et al. MDAnalysis: a Python package for the rapid analysis of molecular dynamics simulations. Proceedings of the 15th python in science conference. 2016; p 105.

[65] Tuckerman, M. E.; Marx, D.; Parrinello, M. The nature and transport mechanism of hydrated hydroxide ions in aqueous solution. *Nature* **2002**, *417*, 925–929.

[66] Marx, D.; Chandra, A.; Tuckerman, M. E. Aqueous basic solutions: hydroxide solvation, structural diffusion, and comparison to the hydrated proton. *Chemical reviews* **2010**, *110*, 2174–2216.

[67] Tian, Y.; Hong, J.; Cao, D.; You, S.; Song, Y.; Cheng, B.; Wang, Z.; Guan, D.; Liu, X.; Zhao, Z., et al. Visualizing Eigen/Zundel cations and their interconversion in monolayer water on metal surfaces. *Science* **2022**, *377*, 315–319.

[68] Halle, B.; Karlström, G. Prototropic charge migration in water. part 2.—Interpretation of nuclear magnetic resonance and conductivity data in terms of model mechanisms. *Journal of the Chemical Society, Faraday Transactions 2: Molecular and Chemical Physics* **1983**, *79*, 1047–1073.

[69] Sluyters, J.; Sluyters-Rehbach, M. The mechanism of the hydrogen ion conduction in liquid light and heavy water derived from the temperature dependence of their limiting conductivities. *The Journal of Physical Chemistry B* **2010**, *114*, 15582–15589.

[70] Chen, M.; Zheng, L.; Santra, B.; Ko, H.-Y.; DiStasio Jr, R. A.; Klein, M. L.; Car, R.; Wu, X. Hydroxide diffuses slower than hydronium in water because its solvated structure inhibits correlated proton transfer. *Nature chemistry* **2018**, *10*, 413–419.

[71] Dang, L. X.; Chang, T.-M. Molecular dynamics study of water clusters, liquid, and liquid–vapor interface of water with many-body potentials. *The Journal of chemical physics* **1997**, *106*, 8149–8159.

[72] Braslau, A.; Deutsch, M.; Pershan, P. S.; Weiss, A.; Als-Nielsen, J.; Bohr, J. Surface roughness of water measured by x-ray reflectivity. *Physical review letters* **1985**, *54*, 114.

[73] McBain, J.; Bacon, R.; Bruce, H. Optical surface thickness of pure water. *The Journal of Chemical Physics* **1939**, *7*, 818–823.

[74] Liu, J.; Yang, J.; Zeng, X. C.; Xantheas, S. S.; Yagi, K.; He, X. Towards complete assignment of the infrared spectrum of the protonated water cluster $H^+(H_2O)_21$. *Nature communications* **2021**, *12*, 6141.

[75] Tian, C.; Ji, N.; Waychunas, G. A.; Shen, Y. R. Interfacial structures of acidic and basic aqueous solutions. *Journal of the American Chemical Society* **2008**, *130*, 13033–13039.

[76] Crespo, Y.; Hassanali, A. Unveiling the Janus-like properties of OH^-. *The Journal of Physical Chemistry Letters* **2015**, *6*, 272–278.

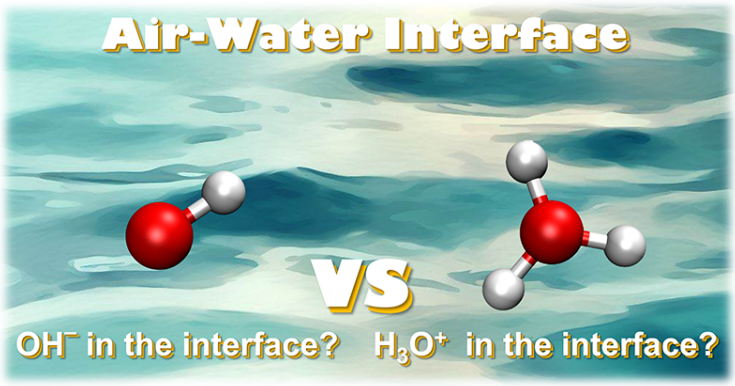

Table of contents (TOC)